

# Synthesis and Characterization of Photocatalytic Material TiO<sub>2</sub>/SBA-15

Nguyen P. Hung<sup>1</sup>, Nguyen T. V. Hoan<sup>1</sup>, Nguyen V. Nghia<sup>2,\*</sup>

<sup>1</sup>Department of Chemistry, Quy Nhon University, Quy Nhon City, Binh Dinh Pro., Vietnam

<sup>2</sup>Department of Physics, Quy Nhon University, Quy Nhon City, Binh Dinh Pro., Vietnam

**Abstract** TiO<sub>2</sub>/SBA-15 materials have been synthesized via a simple indirect hydrothermal method under weak acidic conditions. The powder was characterized by X-ray diffraction (XRD), N<sub>2</sub> adsorption-desorption, Fourier transformed infrared spectroscopy (FT-IR), scanning electron microscopy (SEM) and transmission electron microscopy (TEM). The synthetic products showed highly ordered mesoporous structure with uniform pore sizes, specific surface areas  $S_{BET}$  of 133 m<sup>2</sup>/g and 256 m<sup>2</sup>/g at the TiO<sub>2</sub>:SiO<sub>2</sub> mass ratios of 75:25 and 50:50, respectively. The photocatalytic activity of these materials has been studied by methylene blue decomposition under UV light irradiation.

**Keywords** SBA-15, Titania, Mesoporous Materials, Photocatalytic Materials

## 1. Introduction

The study of TiO<sub>2</sub> nanomaterials as a photocatalyst was started since the invention of two Japanese scientists in 1972 in decomposition of water by photo-electrolysis method over TiO<sub>2</sub> catalyst[1]. Since then, the main areas of research and applications of TiO<sub>2</sub> nanomaterials are: H<sub>2</sub> production by water photodissociation, cleaning toxic air, contaminated water treatment, self-cleaning layer glasses and tissues, killing of bacteria, virus and mold, etc[2-4]. TiO<sub>2</sub> exhibits remarkable advantages including durable material, low cost, environmental friendliness, high photocatalytic activity[5,6]. However, TiO<sub>2</sub> catalysts were prepared by the conventional method has some disadvantages that limit applications in practical, such as low surface area, their photocatalytic activity can exhibit only under the excitation light in ultraviolet region, difficult to separate and recover TiO<sub>2</sub> from aqueous solution.

Recently, many efforts have been made on supporting TiO<sub>2</sub> on porous adsorbents such as mesoporous silica, zeolite, carbon fibers or nanotubes,...[7-13]. As a catalytic support, mesoporous silica has attracted attention due to its high surface area, adjustable pore size, ordered frameworks, and transparent to UV radiation[7]. Among the various mesoporous silica, SBA-15 with highly ordered hexagonal structure, is considered as one of the most prominent catalytic supports due to its interesting features of high surface area (600–1000m<sup>2</sup>.g<sup>-1</sup>), controllable pore diameter

(2–30 nm) and high stability[14,15]. Such mesoporous SBA-15 supported TiO<sub>2</sub> material could take the advantages of both TiO<sub>2</sub> and SBA-15. Some research results in preparation of TiO<sub>2</sub>/SBA-15 materials have been published, such as synthesis indirectly by dispersed TiO<sub>2</sub> onto the silica wall of SBA-15 with the assistance of ultrasound[16], synthesis by wet impregnation method[17,18], by *in situ* method[19], dispersed titanium alkoxide on the surface of SBA-15 in organic solvents[20], titanium alkoxide hydrolysis reaction on SBA-15/COOH surface[21], or directly hydrothermal synthesized[22,23]. The authors have found that the photocatalytic activity under ultraviolet light of TiO<sub>2</sub>/SBA-15 materials could be improved compared to the components or commercial TiO<sub>2</sub> (P25). However, the results of TiO<sub>2</sub>/SBA-15 materials are still only at initial exploration. A suitable synthesis method is desirable for obtaining TiO<sub>2</sub> dispersing on mesoporous silica with high photocatalytic performance. In this paper, we show some results about preparation of TiO<sub>2</sub>/SBA-15 materials by post-synthesis method from titanium alkoxide and as-synthesised SBA-15 and their photocatalytic feature.

## 2. Experimental

### 2.1. Synthesis

Mesoporous silica SBA-15 was synthesised using the triblock copolymer Pluronic P123 (PEO–PPO–PEO, Aldrich) as a surfactant template under acid condition. Typically, 4 g Pluronic P123 template was dissolved in 150 mL of 2 M HCl at 40°C under stirring, followed by addition of 8.5 g of tetraethyl orthosilicate (TEOS, Merck). The resulting mixture was stirred continuously at 40°C for 20h. The

\* Corresponding author:

nguyenvannghia@qnu.edu.vn (Nguyen V. Nghia)

Published online at <http://journal.sapub.org/nn>

Copyright © 2013 Scientific & Academic Publishing. All Rights Reserved

resultant solution was then transferred into a Teflon-lined stainless autoclave and hydrothermally treated at 81 °C for 24 h. After naturally cooling to room temperature, the resultant product was washed, filtered and dried for 10 h at 80 °C in an oven. The white product was calcined at 500 °C for 5 h. This sample is indicated as SBA-15.

TiO<sub>2</sub>/SBA-15 photocatalysts were synthesized using titanium isopropoxide (Ti(OPr)<sub>4</sub>, Merck) and SBA-15 as reactants. 50 ml of isopropyl alcohol used to solubilize titanium isopropoxide was put in a batch well stirred reactor maintained under air atmosphere. SBA-15 pretreated at 80 °C (3 h) in order to remove the adsorbed water, were added to this alcohol under continuous stirring. Then, titanium isopropoxide/alcohol solution was slowly added. After completing the addition of the titanium solution, the reactor was maintained under stirring overnight at room temperature. The mass ratios of TiO<sub>2</sub>:SiO<sub>2</sub> were 25:75, 40:60, 50:50, and 75:25. The solid was then recovered from the solution by filtration, washed and dried at 80 °C for 2 h and finally calcined at 550 °C for 5 h under air. These samples were denoted G13, G23, G11 and G31, respectively.

## 2.2. Characterization

The synthetic materials were characterized by methods including Low Angle X-ray diffraction, Powder X-ray diffraction (XRD Siemen D 5005 Cu-K $\alpha$  radiation), UV-Vis (Varian Lary 5E diode array spectrometer), SEM (Hitachi S4800), TEM (JEOL JEM-1010). The N<sub>2</sub> adsorption-desorption isotherms were measured at -196 °C on a

Qantachorme, Autosorb-1-C sorptometer. The surface areas were calculated by BET equation and the BJH pore size distributions were calculated from adsorption isotherm (ASAP 2010). Fourier transformed infrared (FT-IR) spectra were taken in a Bruker Tensor 27 instrument.

## 2.3. Photocatalytic Activity Measurement

The photocatalytic activity experiments of the prepared TiO<sub>2</sub>/SBA-15 materials were tested for methylene blue (MB) solution photodegradation carried out using a photocatalytic setup that contains a glass reactor and a UV lamp mounted 10 cm away from the reaction solution. The glass reactor holds water circulation facility at the outer wall of it. For a typical photocatalytic experiment, 0.04 g catalyst was mixed with 20 ml of MB solution at concentration of 80 mg.L<sup>-1</sup>. Prior to photodegradation, the catalyst was dispersed in the dark for 30 min to establish adsorption equilibrium. Then the solution was continuously stirred with a magnetic stirrer under UV light irradiation. This solution was withdrawn at given time intervals during the illumination, and immediately centrifuged at 6000 rpm for 15 min. The concentration of MB in solution was determined by recording the absorbance on a UV-Vis spectrophotometer.

# 3. Results and Discussion

## 3.1. X-Ray Diffraction Characterization

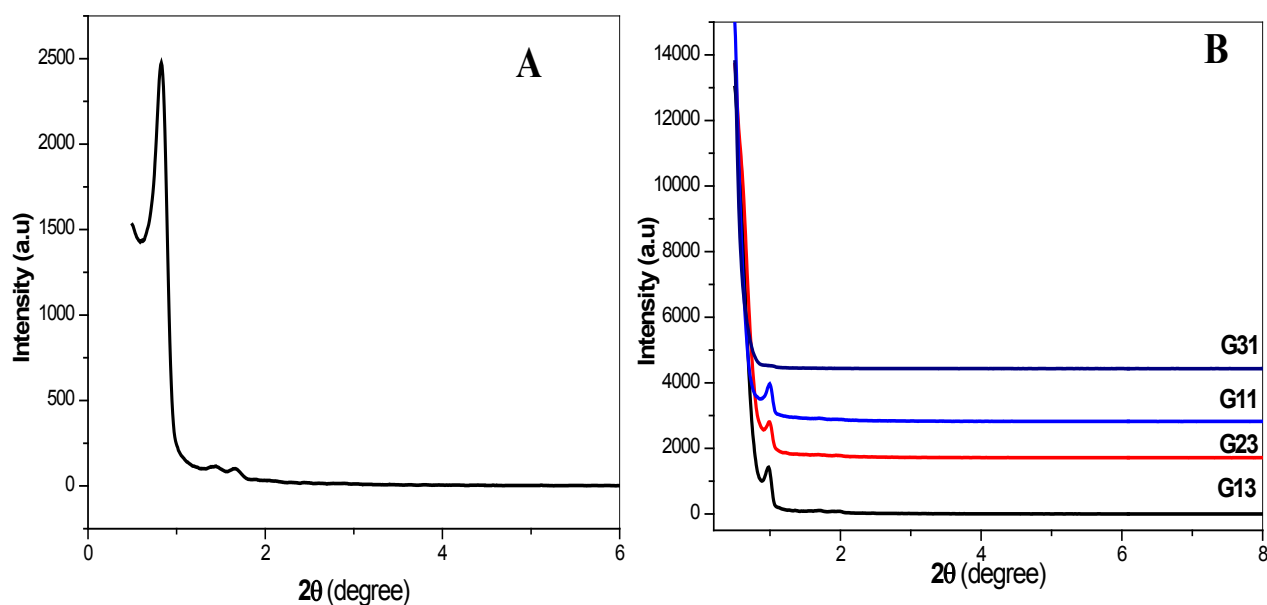
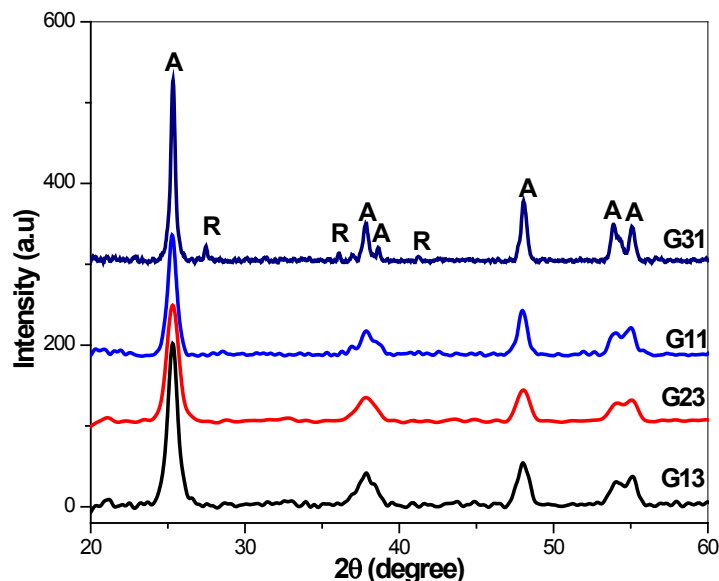


Figure 1. Low angle XRD pattern of SBA-15 (A); Low angle XRD patterns of G13, G23, G11, G31 (B)



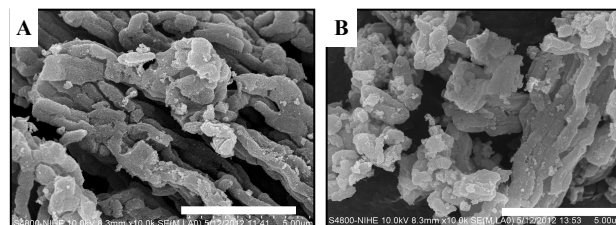
**Figure 2.** Wide-angle XRD patterns of  $\text{TiO}_2/\text{SBA-15}$  synthesized with different  $\text{TiO}_2:\text{SiO}_2$  mass ratios (A: anatase, R: rutile)

Figure 1(A) gives the low angle XRD pattern (LAXRD) of SBA-15. It clearly shows three peaks of (100), (110) and (200) faces, associated with the hexagonal symmetry of mesoporous structure[21]. Figure 1(B) displays the LAXRD patterns of samples G13, G23, G11, G31. All patterns also display three diffraction peaks in the  $2\theta$  range of  $0.5-2^\circ$ , which correspond to the (100), (110) and (200) reflections of the hexagonal mesoporous structure, similar to that observed for the original SBA-15. These results demonstrate that the prepared mesoporous  $\text{TiO}_2/\text{SBA-15}$  materials possess long-range framework ordering and are very stable. The results also showed that after loading  $\text{TiO}_2$ , the intensity of the low angle XRD peaks corresponding to the hexagonal symmetry decreased and shifted slightly to higher angle with increasing  $\text{TiO}_2$  loading indicated the distortion of the mesoporous framework was increased by the intercalated  $\text{TiO}_2$ . The wide angle XRD patterns of  $\text{TiO}_2/\text{SBA-15}$  samples synthesized with different  $\text{TiO}_2:\text{SiO}_2$  mass ratios are shown in Figure 2. It can be seen that the only titania crystalline phase (majority of anatase, minority of rutile) present in all prepared materials. Peak intensity of rutile phase increased with increasing titania content ( $\text{TiO}_2:\text{SiO}_2$  mass ratio from 25:75 to 75:25). The crystallite size ( $d_{\text{XRD}}$ ) of titanium oxide was 10 nm that determined by X-ray analysis for  $\text{TiO}_2$  (101) peaks ( $2\theta = 25.3^\circ$ ) according to the Scherrer formula.

### 3.2. Scanning and Transmission Electron Microscopy Characterization

The morphology of synthesised  $\text{TiO}_2/\text{SBA-15}$  materials is further evident from the SEM and TEM observation. Figure 3 represents the SEM of samples G23 and G11. We can see that these samples revealed cylinders comprised of wheat grain shape particles, which are commonly observed in pure SBA-15 materials. Therefore, based on SEM, there are no morphological differences between the obtained silicas.

TEM analysis of the  $\text{TiO}_2/\text{SBA-15}$  composites are shown in Figure 4. Representative TEM images reveal the following: (i) both the images of the samples show highly ordered hexagonal arrays of the mesoporous with uniform pore size corresponding to the results from LAXRD. The hexagonal structure with estimated pore diameter of 6 nm, and a center-to-center pore distance of around 10 nm is observed; (ii) spherical  $\text{TiO}_2$  nanoparticles are highly dispersed in the interior of the SBA-15 channels. The average  $\text{TiO}_2$  nanoparticle sizes were determined from 10 nm to 20 nm, with a narrow distribution.



**Figure 3.** The SEM images of the samples G23 (A) and G11(B)

### 3.3. Porosity Characterization

Figure 4 is the  $\text{N}_2$  adsorption–desorption isotherms (A) and the corresponding BJH pore size distributions (B) for G11 and G31 samples. The isotherms display an initial steep rise at low partial pressure owing to monolayer nitrogen adsorption followed by a well-defined inflection at higher partial pressure of 0.3 to 0.8 arising from capillary condensation of nitrogen in the framework-confined mesopores. The nitrogen adsorption–desorption isotherms of prepared materials are of type IV with H1-type hysteresis loop (according to classification of IUPAC) that is characteristic of SBA-15. This shows that the doping  $\text{TiO}_2$  do not significantly change structure of SBA-15. The pore size distribution calculated from the desorption branches using the BJH method is shown in Figure 5(B). It is found that samples show a narrow pore size distribution with the

diameter about 5.5 nm. Compared to SBA-15 with the pore size is around 6 nm shows that the doping TiO<sub>2</sub> on SBA-15 leads to decreasing in its pore size. The trend in the pore size distribution indicates that TiO<sub>2</sub> nanoparticles are formed evenly on the surface of SBA-15. More interestingly, the peak of the distribution curve at 5.5 nm of G11 sample is strongest. From N<sub>2</sub> adsorption-desorption data, the BET specific surface area of synthesised TiO<sub>2</sub>/SBA-15 materials

were determined of 133 m<sup>2</sup>/g and 256 m<sup>2</sup>/g at the TiO<sub>2</sub>:SiO<sub>2</sub> mass ratios of 75:25 and 50:50, respectively, those are higher than that of pure TiO<sub>2</sub> powder such as Degussa P25 (just over 50 m<sup>2</sup>/g). Authors in[24,25] also found that, by the conventional hydrothermal method, the loading of titanium dioxide on the framework of SBA-15 makes the pore diameter, the pore volume and the surface area decrease compared to that of SBA-15.

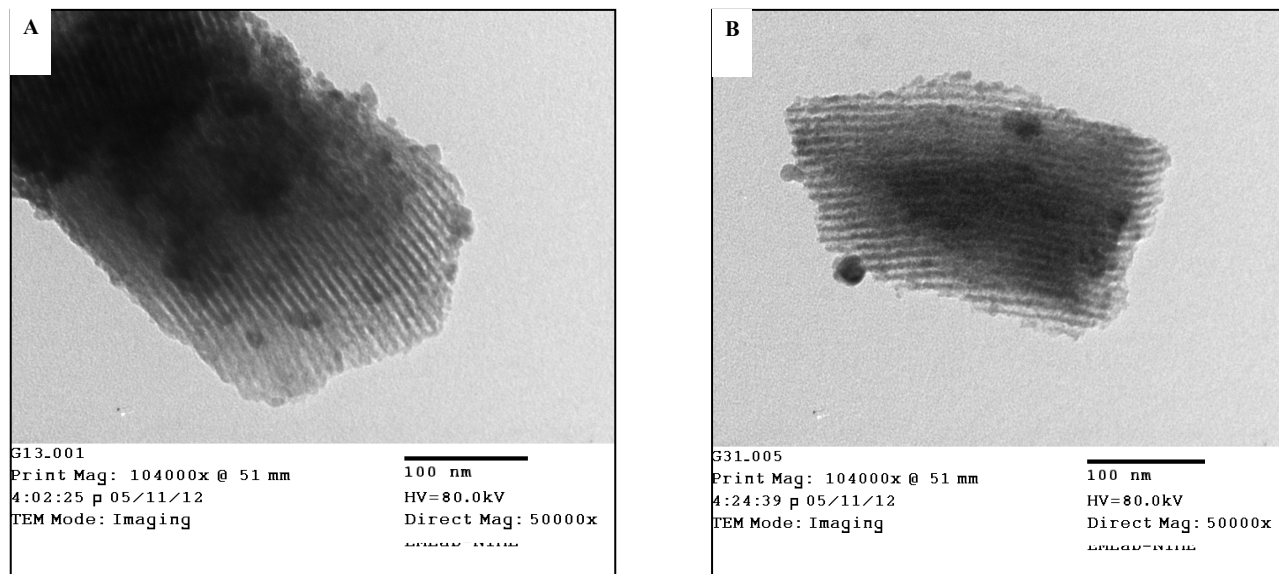


Figure 4. The TEM images of the samples G13 (A) and G31 (B)

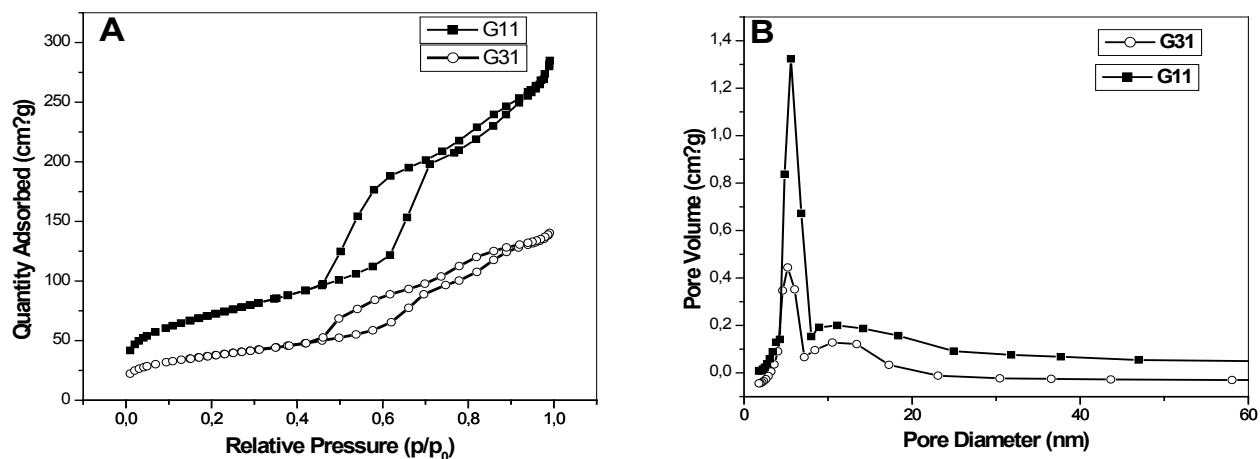


Figure 5. N<sub>2</sub> adsorption-desorption isotherms (A) and the corresponding pore size distributions (B) for G11, G31

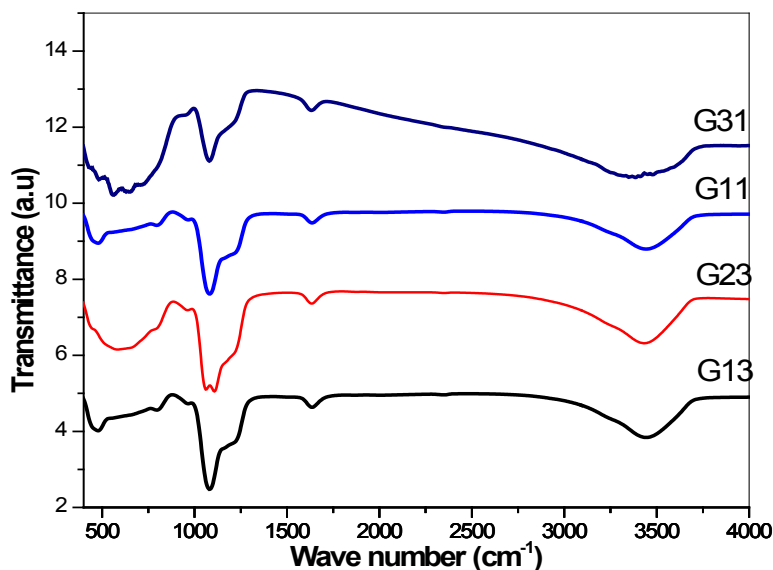


Figure 6. FT-IR spectra of samples G13; G23; G11 and G31

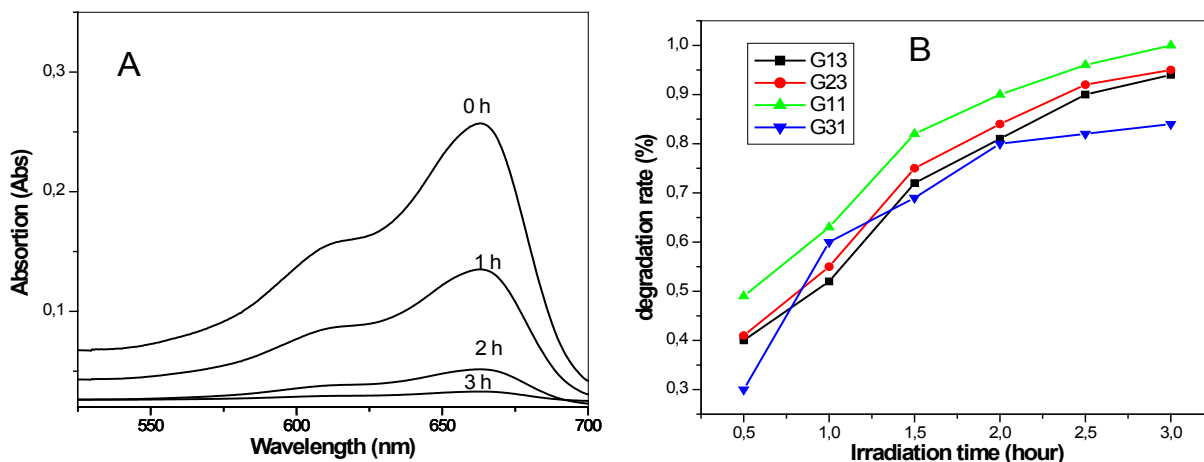


Figure 7. The UV spectra of MB on G11 sample (A) and the conversion of MB on TiO<sub>2</sub>/SBA-15 materials (B) after different irradiation time

### 3.4. Infrared Characterization

FT-IR spectra of the samples calcined at 550 °C for 5 h are shown in Figure 6. In all spectra, the peaks at around 3448 cm<sup>-1</sup> and 1633 cm<sup>-1</sup> can be attributed to the stretching vibration of hydroxyl in surface-adsorbed water and Si-OH or Ti-OH of the mesoporous materials[22]. The peak at 1085 cm<sup>-1</sup> corresponds to the asymmetric stretching vibration of Si-O-Si, and the peaks at 800 cm<sup>-1</sup> and 460 cm<sup>-1</sup> can be assigned to the symmetric stretching and deformation modes of Si-O-Si[26]. As shown in Figure 6, a weak peak at about 960 cm<sup>-1</sup> is observed for all samples. The IR bands observed at 910 cm<sup>-1</sup> – 960 cm<sup>-1</sup> can be assigned to the Si-O-Ti and Si-O-Si stretching vibration[22].

### 3.5. Photocatalytic Activity Test

The photocatalytic activity of synthesised TiO<sub>2</sub>/SBA-15 materials was tested by decomposition reaction of methylene blue (MB) under UV light irradiation. The observed evolution of the UV spectra of MB after different irradiation time is shown in Figure 7(A). When increasing illumination

time, the absorption peak intensity at 630 nm of MB decreased remarkably. Figure 7(B) shows the time course of MB degradation by the mesoporous TiO<sub>2</sub>/SBA-15 composite photocatalysts with TiO<sub>2</sub> content ranging of 25–75 wt%. The TiO<sub>2</sub>/SBA-15 mesoporous materials prepared with the TiO<sub>2</sub>:SiO<sub>2</sub> mass ratios of 25:75, 40:60, 50:50 reveal high photocatalytic degradation rates, MB was decomposed more than 90% after 2.5 hours. The G11 sample (TiO<sub>2</sub>:SiO<sub>2</sub> mass ratio of 50:50) expressed the best photocatalytic activity. This is agreement with the results of XRD and the N<sub>2</sub> adsorption-desorption. The above experimental results showed that the TiO<sub>2</sub>:SiO<sub>2</sub> mass ratio of 50:50 is suitable for the preparation of TiO<sub>2</sub>/SBA-15 nanomaterials having the best photocatalytic activity. The results also showed that, the photocatalytic activity of prepared TiO<sub>2</sub>/SBA-15 composites is much higher than commercial pure TiO<sub>2</sub> nanoparticles. This shows the potential application of photocatalytic ability of TiO<sub>2</sub>/SBA-15 mesoporous materials in pollutant organic compounds treatment. Preparing by hydrothermal loading TiO<sub>2</sub> on SBA-15, authors in[24] found that, their photocatalytic activity for decomposition of methylene blue

increases with increasing TiO<sub>2</sub> loading ratio, shows a maximum value at 7% TiO<sub>2</sub>/SBA-15, and then decreases at 10% TiO<sub>2</sub>/SBA-15.

## 4. Conclusions

The TiO<sub>2</sub>/SBA-15 nanomaterials were synthesized successfully by post-synthesis method from titanium alkoxide and as-synthesised SBA-15. The structure of synthesised materials includes spherical TiO<sub>2</sub> (majority of anatase, minority of rutile) nanoparticles with average sizes of 10 nm to 20 nm distributed over ordered hexagonal mesoporous SBA-15 support with pore diameter of 5.5 nm. The specific surface areas  $S_{\text{BET}}$  are 133 m<sup>2</sup>/g and 256 m<sup>2</sup>/g at the TiO<sub>2</sub>:SiO<sub>2</sub> mass ratios of 75:25 and 50:50, respectively. The synthesised TiO<sub>2</sub>/SBA-15 nanomaterials express high photocatalytic activity for decomposition reaction of methylene blue, that shows potential application of their photocatalytic ability in pollutant organic compounds treatment.

## ACKNOWLEDGMENTS

This work was supported in part by the Grant-in-Aid for Scientific Research from the Ministry of Education and Training, Vietnam (Project code number B2012.28.47).

## REFERENCES

- [1] Fujishima A, Honda K, "Electrochemical photolysis of water at a semiconductor electrode", *Nature* 37 238, 1972.
- [2] Gaya U I and Abdullah A H, "Heterogeneous photocatalytic degradation of organic contaminants over titanium dioxide: A review of fundamentals, progress and problems", *Journal of Photochemistry and Photobiology C: Photochemistry Reviews* 9 (1) 1-12, 2008.
- [3] Zhang Z, Wang C C, Zakaria R, and Ying J Y, "Role of particle size in nanocrystalline TiO<sub>2</sub>-based photocatalysts", *J. Phys. Chem. B* 102 (52) 10871-10878, 1998.
- [4] Bahnemann D, "Photocatalytic water treatment: solar energy applications", *Sol. Energy* 77 445, 2004.
- [5] Frindell K L, Bartl M H, Popitsch A, Stucky G D, "Sensitized luminescence of trivalent europium by three-dimensionally arranged anatase nanocrystals in mesostructured titania thin films", *Angew. Chem. Int. Ed.* 41 959, 2002.
- [6] Reisner E, Powell D J, Cavazza C, Fontecilla-Camps J C, and Armstrong F A, "Visible light-driven H<sub>2</sub> production by hydrogenases attached to dye-sensitized TiO<sub>2</sub> nanoparticles", *J. Am. Chem. Soc.* 131 18457-18466, 2009.
- [7] Morris D, Egdell R G, "Application of V-doped TiO<sub>2</sub> as a sensor for detection of SO<sub>2</sub>", *J. Mater. Chem.* 11 3207, 2001.
- [8] Gole J, Burda C, Fedorov A, White M, "Enhanced reactivity and phase transformation at the nanoscale: efficient formation of active silica and doped and metal seeded TiO<sub>2-x</sub>N<sub>x</sub> photocatalysts", *Adv. Mater. Sci.* 5 265, 2003.
- [9] Newalkar B L, Olanrewaju J, Komarneni S, "Microwave - hydrothermal synthesis and characterization of zirconium substituted SBA-15 mesoporous silica", *Chem. Mater.* 13 552, 2001.
- [10] Zhu H Y, Othman J A, Li J Y, Zhao J C, Churchman G J, Vansant E F, "Novel composites of TiO<sub>2</sub> (anatase) and silicate nanoparticles", *Chem. Mater.* 14(12) 5037-5044, 2002.
- [11] Zanjanchi M A, Golmojeh H, Arvand M, "Enhanced adsorptive and photocatalytic achievements in removal of methylene blue by incorporating tungstophosphoric acid-TiO<sub>2</sub> into MCM-41", *J. Hazard Mater.* 169(1-3) 233-239, 2009.
- [12] Atsushi K, Takashi G, Katsumi K and Takayuki T, "Structural and optical characteristics of TiO<sub>2</sub> nanoparticles-containing mesoporous silica (SBA-15) thin films", *IOP Conf. Ser.: Mater. Sci. Eng.* 24 012019, 2011.
- [13] Li Y, Li N, Tu J, Li X, Wang B, Chi Y, Liu D, Yang D, "TiO<sub>2</sub> supported on rod-like mesoporous silica SBA-15: preparation, characterization and photocatalytic behaviour", *Materials Research Bulletin* 46(12) 2317-2322, 2011.
- [14] Rahmat N, Abdullah A Z, Mohamed A R, "A review: Mesoporous Santa Barbara Amorphous-15, types, synthesis and its applications towards biorefinery production", *American Journal of Applied Sciences* 7 (12) 1579-1586, 2010.
- [15] Taguchi A, Schuth F, "Order mesoporous materials in catalysis", *Microporous and Mesoporous Materials* 77 1-45, 2005.
- [16] Zhu S, Zhang D, Zhang X, Zhang L, Ma X, Zhang Y, Cai M, "Sonochemical incorporation of nanosized TiO<sub>2</sub> inside mesoporous silica", *Microporous and Mesoporous Materials* 126 20-25, 2009.
- [17] Jing M, Jia C, Liang-sheng Q and Juanqin X, "Synthesis and structural characterization of novel visible photocatalyst Bi-TiO<sub>2</sub>/SBA-15 and its photocatalytic performance", *RSC Adv.* 2 3753-3758, 2012.
- [18] Jing M, Liang-Sheng Q, Han-Yang L, Xiang-Bo T, "A rapid and facile method for synthesis of TiO<sub>2</sub>/SBA-15 and its photocatalytic application", *Science of Advanced Materials*, 2(4) 539-544, 2010.
- [19] Witte K D, Busuioac A M, Meynen V, Mertens M, Bilba N, Tendeloo G V, Cool P, Vansant E F, "Influence of the synthesis parameters of TiO<sub>2</sub>-SBA-15 materials on the adsorption and photodegradation of rhodamine-6G", *Microporous and Mesoporous Materials* 110 100-110, 2008.
- [20] Perathoner S, Lanzafame P, Passalacqua R, Centi G, Schlögl R, Su D S, "Use of mesoporous SBA-15 for nanostructuring titania for photocatalytic applications", *Microporous and Mesoporous Materials* 90 347-361, 2006.
- [21] Zhang S, Jiang D, Tang T, Li J, Xu Y, Shen W, Xu J and Deng F, "TiO<sub>2</sub>/SBA-15 photocatalysts synthesized through the surface acidolysis of Ti(OnBu)<sub>4</sub> on carboxyl-modified SBA-15", *Catalysis Today* 158 329-335, 2010.
- [22] Qiao W T, Zhou G W, Zhang X T, Li T D, "Preparation and

photocatalytic activity of highly ordered mesoporous TiO<sub>2</sub>-SBA-15”, *Materials Science and Engineering C* 29 1498-1502, 2009.

- [23] Chen Y, Huang Y, Xiu J, Han X, Bao X, “Direct synthesis, characterization and catalytic activity of titanium-substituted SBA-15 mesoporous molecular sieves”, *Applied Catalysis A: General* 273 185–191, 2004.
- [24] Jung W Y, Lim K T, Park S S, Lee G D, Hong S S, “Synthesis of TiO<sub>2</sub> supported on SBA-15 using chelating method and their photocatalytic decomposition of methylene blue”, *J. Nanosci Nanotechnol.* 11(1) 833-837, 2011.
- [25] Jung W Y, Lee G D, Park S S, Lim K T, Lee M S, Hong S S, “Synthesis of TiO<sub>2</sub> supported on SBA-15 using different method and their photocatalytic activity”, *J. Nanosci Nanotechnol.* 11(8) 7446-7450, 2011.
- [26] Yang H C, Lin H Y, Chien Y S, Wu J C S, Wu H H, “Mesoporous TiO<sub>2</sub>/SBA-15, and Cu/TiO<sub>2</sub>/SBA-15 composite photocatalysts for photoreduction of CO<sub>2</sub> to methanol”, *Catal Lett* 131 381-387, 2009.